The work provides the more comprehensive development of Liquid Smoke from Rice Husks Ash (RHA). Notably, the study focuses on the interaction between the primary molecules of inhibitor and mild steel, including thermodynamic calculation and surface treatment upon addition of inhibitor. The electrochemical impedance spectroscopy (EIS) and potentiodynamic polarization (PP) characterization were utilized to evaluate the anticorrosion of RHA. The Raman Spectroscopy pre and post-addition of RHA's inhibitor were used to compare the adsorbed functional group of inhibitors. Moreover, the thermodynamic calculation of the inhibitor's adsorption determines the types of adsorption of the inhibitor. As a result of the adsorption process, the Scanning Electronic Microscope-Energy Dispersive X-Ray (SEM-EDX) aided by The Atomic Force Microscopy (AFM) and Contact Angle Test was implemented to unveil the surface treatment and the change of elemental composition after the addition of an 80 ppm inhibitor. The PP and EIS results show a significant depression of the current density at –2.75 μA•cm^2 in 80 ppm solution with the highest inhibition efficiency of 99.82 %. The superior inhibition correlates to the adsorption of Si–OH, C–C, C–O–C, >C=O, complex structure, and –OH at wavenumber 458, 662, 1095, 1780, and 3530 cm^{-1}. The LS shows a significant surface area of protection of 0.9982 and high adsorption constant (Kads) at 11.648. The calculated ΔGads of –6.59 kJ/mol unveils the chemisorption in nature. At the same time, a combination of 20 and 80 ppm solution is predicted adsorbed horizontally to reduce the contact between the solution and substrate, as shown in SEM and AFM results. It also increases the contact angle and their corresponding hydrophobicity

Keywords: liquid smoke, green corrosion inhibitor, rice husks ash, chemisorptions

UDC 372
DOI: 10.15587/1729-4061.2022.265086

UNRAVELING THE STUDY OF LIQUID SMOKE FROM RICE HUSKS AS A GREEN CORROSION INHIBITOR IN MILD STEEL UNDER 1 M HCL

Agus Kaban
Master of Engineering, Graduate Student*
Wahyu Mayangsari
Master of Engineering, Researcher**
Mochammad Anwar
Master of Science, Senior Researcher**
Ahmad Maksum
Doctor of Engineering, Lecturer
Research Center for Eco-Friendly Technology
Department of Mechanical Engineering
Politeknik Negeri Jakarta
Jl. G.A. Siwabessy Kampus Baru UI, Depok, Indonesia, 16425
Taufik Aditiyawarman
Master of Science, Graduate Student*
Johny Soedarsono
Doctor of Engineering, Professor*
Aga Ridhova
Master of Engineering, Researcher
Research Center for Metallurgy-National Research and Innovation Agency
KST B.J. Habibie, Tangerang Selatan, Indonesia, 15314
Rini Riastuti
Corresponding author
Doctor of Engineering, Senior Lecturer*
E-mail: riastuti@metal.ui.ac.id
*Prof Johny Wahyuadi Laboratory
Department of Metallurgical and Materials Engineering
Universitas Indonesia
Kampus Baru UI Depok, Jawa Barat, Indonesia, 16424
**Research Center for Metallurgy-National Research and Innovation Agency
KST B.J. Habibie, Tangerang Selatan, Indonesia, 15314

Received date 18.07.2022
Accepted date 16.09.2022
Published date 30.10.2022

How to Cite: *Kaban, A., Mayangsari, W., Anwar, M., Maksum, A., Aditiyawarman, T., Soedarsono, J., Ridhova, A., Riastuti, R. (2022). Unraveling the study of liquid smoke from Rice Husks as a green corrosion inhibitor in mild steel under 1 M HCl. Eastern-European Journal of Enterprise Technologies, 5 (6 (119)), 41–53. doi: https://doi.org/10.15587/1729-4061.2022.265086*

1. Introduction

Pipelines are the heart of the oil and gas distribution to ensure the energy products meet society and industrial activities. Despite considering the most prominent way to transport the source of energy [1], the material remains susceptible to corrosion. Yearly, the oil and gas company allots nearly USD 1400 to reconstruct the risk of corrosion [2] and requires an additional USD 2.5 trillion to adverse the effect of corrosion as reported in [3]. In industry, acidic pickling

removes unwanted substances in which, at lower pH, the metal's dissolution under an acidic environment causes corrosion and lowers the mechanical properties of the metal. Therefore, protection against corrosion is the tradeoff to incorporating pipeline maintenance and ensuring a continuous energy supply [4, 5]. Corrosion classification includes galvanic corrosion, stray current corrosion, and corrosion related to the cell's concentration, demonstrating that the electrochemical process is critical in the oil and gas industries.

Although corrosion is a natural electrochemical process, it allows the metals and alloys to achieve their thermodynamic stability in oxides [6], such as Fe_2O_3 and Fe_3O_4. Corrosion occurs when metals are in contact physically and chemically with their environment and lower materials' integrity. In addition, it develops and induces internal corrosion defects in pipelines [7] despite the variation of operating pressure, the characteristic of fluids, and the injection inhibitors system. Several approaches have been implemented to address the risk of corrosion, such as cathodic protection [8], coatings [9], selection of materials [10], and injection of corrosion inhibitors [11–13]. The primary objective of handling corrosion (corrosion management) is to understand how to reduce the corrosion rate. One of the practical and affordable solutions to resolve the issue is the introduction of a corrosion inhibitor (CI).

In the last decade, there has been a tremendous effort in harnessing the potential of plants to replace the commercial inorganic CI (nitrite based), which has been effectively proven to protect the reinforcing bar or steel [14]. Several published works have elaborated on the formation and evolution of passive film with their protection. The research of [15] argues the carbon steel of API 5L Grade B can be an excellent choice to reduce the corrosion effect using Secang heartwood (*caesalpinia sappan l*) under a 3.5 % NaCl solution. Although the selection of natural inhibitors successfully inhibits corrosion activities, the inhibitor remains inadequate to protect the bare metal due to low inhibition efficiency of 53.18 %, according to potentiodynamic polarization measurements. The limitation of the research was addressed by the introduction of *Morinda citrifolia* [16] and fitted the requirement for low carbon steel protection under the same solution. The work reports an improvement in inhibition of nearly 77 %, with the lowest corrosion rate of 1.385 mpy. Meanwhile, the published research [17] reveals that sweet potato extract's additional effect impairs ascorbic acid's shortcoming as a corrosion inhibitor due to its feasibility of being oxidized in solution. All of these examples of research constitute the ability of organic contents of plant to establish chemical bonding with metals. Notably, the highly electronegative atoms of S, O, N, P, and the presence of π and σ bonds are critical to strengthening the adsorption molecules on the surface of metals [18].

In the last decade, a few publications have been developed to harness the potential of rice husks ash (RHA) as green corrosion inhibitors to mitigate the general corrosion of mild steel. The primary consideration for using RHA as green corrosion inhibitor is low cost and is classified as waste products. A few publications showcase using RHA as a coating material for mild steel exteriors under chloride environments [19]. In their work, the RHA was embedded into the composite of Zn-ZnO-XRHA using the electrodeposition technique to give 96 % inhibition efficiency. Our previous research [20] has shown the anticorrosion of RHA on mild steel under 1M HCl corresponds to the bioactive functional group of the inhibitor. However, there has been little success in incorporating the actual RHA bioactive composition with their nature of adsorption to influence high inhibition efficiency. It also remains challenging to determine the effect of surface treatment on mild steel as a higher inhibitor dosage response at elevated temperature on an atomic scale related to their hydrophobicity. The spectroscopy study of Raman to unveil the functional group's contribution before and after the adsorption of inhibitors is used to address the issue. Moreover, the utilization of Gas Chromatography-Mass Spectroscopy (GCMS) aided by the comprehensive elucidation of the Atomic Force Microscopy (AFM) characterization and Contact Angle measurement have been made to confirm the adsorption process. Therefore, research on the development of LS in RHA using the above characterization and calculation is relevant to ease an advance study on how to harnessing the potential of inhibitor at numerous parameters.

2. Literature review and problem statement

Corrosion inhibitors are chemicals commonly utilized to achieve protection not limited to the internal layer of pipelines to minimize the electrochemical reaction. The paper [21] shows GCI works by modifying the surface of metals, and the surface treatment of the inhibited surface is associated with the adsorption of an inhibitor's protective film. Except for the source types of inhibitor, the heteroatoms of N, P, S, and O and the corresponding functional groups such as $-OH$, $-SH$, NH_2, $-OCH_3$ are commonly present in natural inhibitors. The above molecules and functional groups often appear in organic inhibitors to reduce the harmful effect of several synthetic corrosion inhibitors based on chromate, nitrite, and benzoate compounds [22]. As such, the recent research on developing green corrosion inhibitors has massively harnessed, which generally are more water soluble and retain a lower risk to the environment upon disposal. A few papers have elaborated on the use of corrosion inhibitors to lengthen the metal's protection. The paper of [23] uses *Pluchea indica* Less. Leaves extract to protect low carbon steel under 3.5 % NaCl solution. According to the characterization of weight loss and polarization results, the optimum inhibitor value of 3 mL depresses the corrosion rate of the metal when it dissolves for 216 hours. Despite the low volume of inhibitors used, there is an unresolved problem related to determining the most influential functional groups which affect the adsorption on the surface of the substrate. This difficulty may correlate to inhibitor molecules' complexity and provides inaccurate corrosion mitigation of the inhibitor.

The work of [24] studies the use of *Eleutherine Americana Merr.* Extract to analyze the plant to suppress the electrochemical reaction related to corrosion on the API 5L X42 substrate under acidic conditions. It shows that the corrosion inhibition achieved the highest protection when a 1000 ppm solution was added. The reported FTIR spectrum shows the content of the inhibitor mainly originated from the flavonoid. However, the shortcomings of the research constitute the lack of characterization techniques to obtain the primary molecules which facilitate the inhibition process. Furthermore, the work is inadequate to discuss the rapid changes of surface post addition of inhibitors and the dramatic reduction in hydrophilicity measurements of the working electrode.

An option to overcome the relevant difficulties can be tested using spectroscopy techniques, thermodynamics calculations, and extensive analysis in surface treatments. This is the approach used in the recent work of [25] that briefly elaborated on the use of Dardagan fruit as an inhibitor using electrochemical and surface morphology to unveil the protection ability of the plant. The researchers report that the 3000 ppm inhibitor is required to achieve 97 % inhibition efficiency at 6 hours of immersion substrate time. A slight improvement was offered by the work of [26] that utilizes the *Chinese gooseberry* fruit shell extract to evaluate the corrosion inhibitory performance of the mentioned plant extract. In their work, AFM, SEM–EDX and contact angle tests were utilized to obtain the relationship between concentration and immersion time. They argued that the concentration of 1000 ppm inhibitor effectively eases corrosion protection, which aligns with the research [27]. Both works showcase the importance of calculating the thermodynamics parameter to determine the adsorptive behavior of the inhibitor (physisorption or chemisorption). A report by [28] highlights the adsorption of the inhibitor to form a barrier of protection through a chemisorption reaction. This reaction is an interaction between the adsorbate and the substrate so that the electron donation occurs to give stronger bonding and reduction capability of inhibitor.

In this previous work, adsorptive implementation of GCI on the surface of mild steel inherent several limitations. The initial study was inadequate to discuss, the actual composition of RHA inhibitor molecules which accountable for the adsorption process, the nature of adsorption of RHA inhibitor (chemisorption or physisorption), and to explain the sharp reduction in terms of hydrophilicity of inhibitor. The above restrictions make the relevant information of RHA research impractical. This is the approach used in [29], where the adsorption of certain functional groups gives valuable information regarding how the inhibitor replaces the water molecules from the substrate. However, this study remains unclear as to explain the use of liquid smoke which may quicken the adsorption process. All this allows to argue that it is appropriate to conduct a study devoted to unveiling the actual molecule's contributions in the adsorption process.

3. The aim and objectives of the study

The aim of the study is to unveil the relationship between the actual bioactive molecules of RHA to their adsorption process on mild steel under HCl 1M. This will make it possible to a provision in controlling the corrosion threat in oil pipelines through the evaluation of inhibitors.

To achieve this aim, the following objectives are accomplished:

– to identify the primary bioactive molecules in LS of RHA and their anticorrosion behavior, which involves in the adsorption process;

– to elaborate on the contribution of actual functional groups before and after the addition of inhibitors;

– to determine the nature of adsorption of the inhibitor (chemisorption or physisorption);

– to study the surface morphology of the mild steel, including surface roughness and its hydrophobicity.

4. Materials and methods

4. 1. Object and Hypotheses of the study

The source of Liquid Smoke (LS) of RHA was taken from the local farmer in West Java, Indonesia. The amount of rice husk ash purchased was about 1 kg. It is predicted that the phenolic compounds and their respective π-bonding system in the complex structure of LS provide excellent inhibition due to the formation of the passive film. It correlates to the longest diameter of Nyquist and the depression of $i_{corr,}$ which lowers the likelihood of the dissolution of the metal under a lower pH solution. It is also predicted that the C=O, C–O–C, complex structure of benzene, and Si–O bonds increase the adsorption of metals by expanding the surface charged between the metals and LS inhibitors.

4. 2. The Chemical and Materials

As previously published, the LS inhibitor was prepared using pyrometallurgy to convert the fifty grams of rice husks (RH) into an inhibitor solution [20]. The selection technique was made according to the characteristic of rice husk Physico-chemical from being completely extracted from the plant and quickening the production on a large scale at an affordable operational cost. The prepared inhibitor solution was prepared with 1 M HCl solution. The acidic solution was diluted using distilled water from the original 37 % standard solution of HCl (Merck Co) to prepare 0, 20, 40, 60, and 80 ppm RHA inhibitor solutions. The chemical composition of mild steel was iron (62.72 %), carbon (0.062 %), chromium (0.011 %), sulfur (0.059 %), manganese (0.1698 %), nickel (0.0145 %), tin (0.0017 %), and vanadium (0.0029 %).

4. 3. Electrochemical and Polarization Test

The electrochemical measurements were conducted using Gamry Instrument G750 (United States) with an electrochemical analyzer. Three glasses set up a cell to evaluate the corrosion mitigation of the inhibitor. The working electrode was prepared by removing the oxide layer with a cross-sectional area of 1 cm^2. The mounted mild steel electrode was immersed in a blank solution (1 M HCl) to achieve the potential of a steady-state open circuit (E_{ocp}) for 60 minutes for each measurement. The counter electrode was Platinum (Pt), having a surface area of 1 cm^2. On the other hand, the saturated calomel electrode (SCE) of Ag/AgCl (Metrohm, Switzerland) was used as a reference electrode in which the potential measurement of EIS was based on the electrode. The Potentiodynamic polarization was measured between –200 and +200 mV versus SCE using a 1 mV/s scanning rate. The Tafel Polarization and EIS curves explained the LS's inhibitive action.

4. 4. Gas Chromatography-Mass Spectroscopy analysis

The Gas Chromatography-Mass Spectroscopy analysis was conducted considering the relevance between the inhibitor molecules and the inhibitive behavior of the primary molecule. The method combines several gas chromatography features and mass spectroscopy to identify various substances in the LS. The qualitative and quantitative LS compounds were carried out using Agilent 7890B (GC) types 19091S-433 (United States) using 5 % phenyl methyl siloxane non-polar column and 5977A (MS) methods to injection volume of inhibitor was one μL. The

thermal process was carried out at an initial temperature of 40 °C (symbol already), a hold time of 1 minute, and a post-run temperature of 300 °C. Through LS's retention time and corresponding mass spectra evaluation to the mass spectral databases of WILEY 09 and NIST 11, the molecule dominant of LS's molecules was separate, purified, and identified.

4. 5. Raman Spectroscopy

The interaction between the corresponding functional group of the primary inhibitor molecules and the metal surface before and after immersion was obtained using a modular Raman spectroscopy of iHR320 (Japan) with a CCD detector of 1.024×256 pixels and 785 nm excitation line of a diode laser. The control spectrum variable was the spectra of uninhibited mild steel. Another spectrum was collected with an exposure of mild steel upon dissolution in 80 ppm LS solution. Before obtaining the Raman spectra, the substrate was allowed free from air interaction after immersion with distilled water.

4. 6. Surface treatment analysis

The surface morphology of untreated and treated substrates unveiled the inhibitor activity. The electronic scanning microscope (SEM) was used using JEOL JSM 6390 (Japan) with complimentary EDX analysis to determine the composition of elements in the film. The mild steel substrate was prepared into a 1 cm^2 shape at 20 kV accelerated voltage. The distribution of damaged surfaces was studied using particle analysis which will be further used as a label in Machine Learning studies. Moreover, the AFM of NX10 Atomic Force Microscopy Park System (South Korea) was utilized to obtain film roughness and skewness parameter. This parameter was used to determine the surface roughness of uninhibited metals. In addition, the contact angle measurement of the Osila Contact Angle Instrument (United Kingdom) was used to explain the nature of the hydrophobicity of mild steel. 0.2 cm^3 of distilled water was dropped on the surface of the metal and immersed for one week in an 80 ppm solution. The improvement of contact angle is associated with the adhesion force to describe the molecular interaction between the inhibited and non-inhibited surface.

5. Research results of liquid smoke as a green corrosion inhibitor

5. 1. Anticorrosion behavior test and primary bioactive molecules results

5. 1. 1. The Potentiodynamic Polarization and Electrochemical Impedance Spectroscopy results

The effect of LS from RHA as a GCI on the polarization behavior of mild steel in 1 M HCl was evaluated as depicted in the Tafel graph and was obtained at multiple concentrations (Fig. 1, *a*).

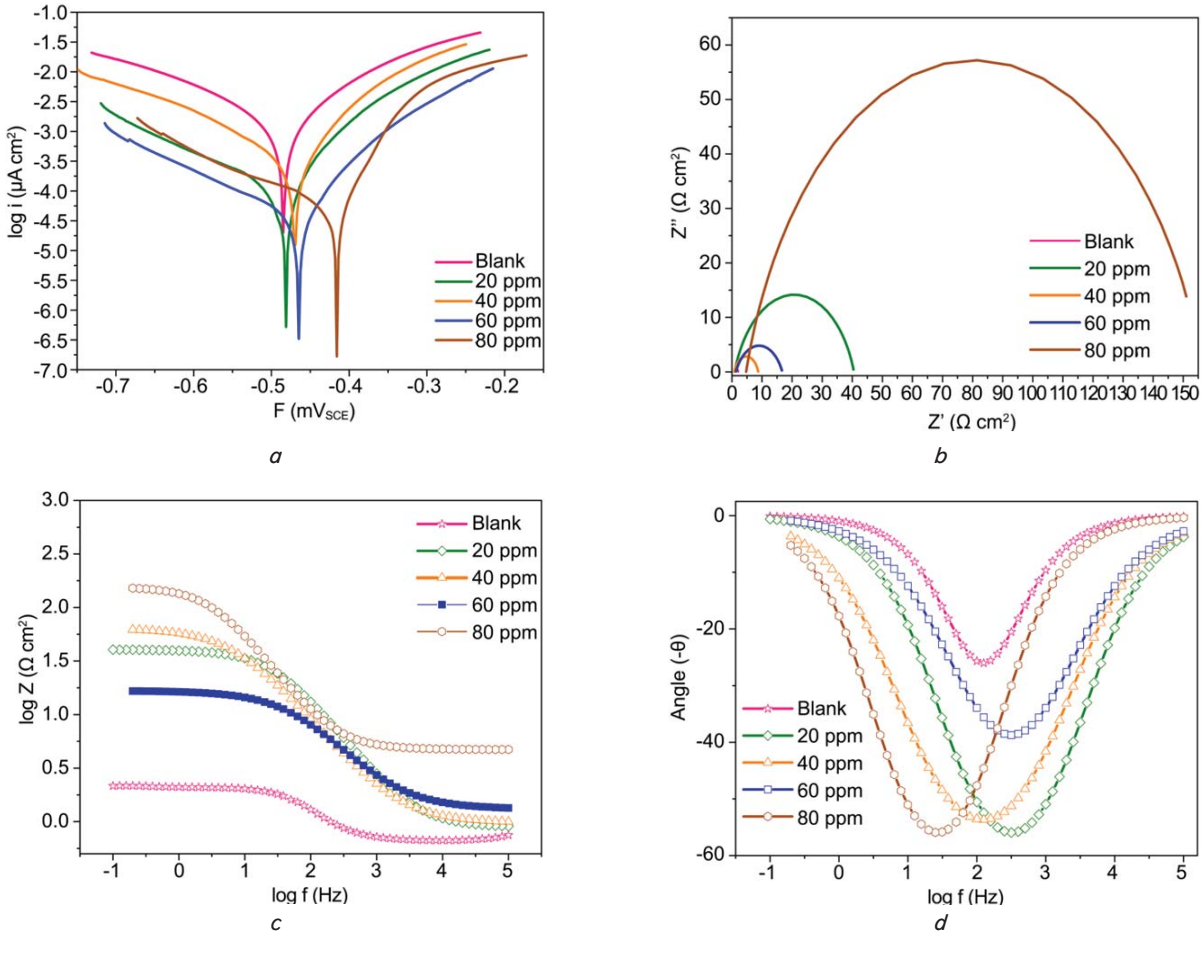

Fig. 1. The result of anticorrosion behavior: *a* — Tafel Polarization; *b* — Nyquist Plot; *c* — Bode Plot; *d* — Bode Angle

Fig. 1, *a* shows a shift for cathodic and anodic branches to a lower corrosion current density (i_{corr}) and higher corrosion potential (E_{corr}). The mild steel substrate was allowed to immerse in the test solution (LS inhibitor+1M HCl) for various inhibitor concentrations and temperatures of the system before the polarization curves were recorded, starting from potential ranges of the cathodic to anodic. Fig. 1, *a* shows a shift for cathodic and anodic branches to a lower corrosion current density (i_{corr}) and higher corrosion potential (E_{corr}). Compared to unprotected metal, the E_{corr} value of the protected metals move towards the right-hand side. The blank solution has a high corrosion potential of −0.5 mV, and as the concentration of inhibitor increases, the value continuously decreases to nearly −0.4 mV at 80 ppm. At the same concentration, the depression of electrochemical activities decreases the current density to approximately −7 μA. This fact aligns with the Nyquist diagram for mild steel immersed in HCl 1M with and without LS inhibitor. In the beginning, the Nyquist semicircle diameter is smaller for the blank solution than for the solution containing 20–80 ppm. However, it is evident that at the concentration of 40 and 60 ppm solution, the diameter is smaller than 20 and 80 ppm at 10 and 18 Ω cm^2 (Fig. 1, *b*). In addition, Fig. 1, *c, d* report the same result of the same concentration inadequacy to protect the metal by giving lower impedance of 1.3 and 1.6 Ω cm^2 and phase angle at −40° and −55°. On the contrary, the increased concentration of 80 ppm is proportional to the increasing protective effect of the inhibitor.

The corrosion behavior of mild steel under the acidic condition in the absence and the presence of LS inhibitor was evaluated using EIS as depicted in Fig. 1, *b–d*. The method is suitable for characterizing the interaction between inhibitor and substrate due to its reliability and reproducibility, as previously reported by [26]. The result of the Nyquist plot is in good agreement with the Tafel Polarization Curve, while the effect of the calculated EIS parameter is illustrated in Table 1.

Table 1 presents the result of electrochemical parameters at various concentrations and temperatures without and with the inhibitor of LS. It also lists the inhibition efficiency values determined using (1):

$$\left\{\eta = \frac{R_{inh} - R_{ct}^0}{R_{inh}} \times 100\,\%\right\}. \quad (1)$$

In the above equation R_{ct}^0 is the blank solution resistance, R_{inh} is the charge transfer resistance. Both variables have the unit of Ω cm^2. The concentration of 80 ppm (50 °C) gives the optimum protection on the surface of metal due to the highest R_{inh} of 834.9 Ω cm^2. Nevertheless, the result is not only provided in the Nyquist plot (Fig. 1, *b*) but also enlisted in Table 1 more clearly. For the blank solution, the R_{inh} was only 4.87, 2.576, and 1.431 Ω cm^2. Adding LS inhibitor causes the gradual rise in the charge transfer resistance to 243.7, 264.8, and 834.9 Ω cm^2. The result indicates the adsorbed film has excellent protection capabilities.

Furthermore, each CPE system's passivity of Y_o and n of the solution increases. In this work, the value of n predicts the inhibitor's capacitance or resistance. A value of n closer to 0 increases the inhibitor resistance, while the interval of 0–1 enhances the capacitance of the inhibitor [27]. The impedance of the modulus plot and phase angle graph in blank solution and the LS inhibitor at various concentrations are provided in Fig. 1, *c, d* and fit the electrical equivalent circuit (Fig. 2).

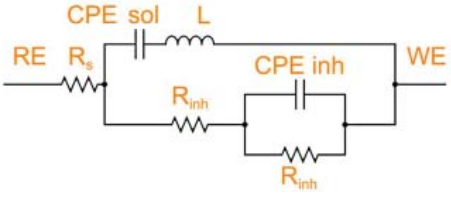

Fig. 2. The Electrical Equivalent circuit

Fig. 2 reveals the presence of double layer impedance due to LS inhibitor adsorption composes a more capacitive passive layer and is provided by the presence of solution and inhibitor Constant Phase Element (CPE). At low frequency, the value of log Z increases, indicating that a higher inhibitor dose in the interface between the mild steel and LS solution shows a typical ideal capacitor [28]. This result agrees with the observable one-time constant of the Bode plot and correlates to the presence of an electric double layer. Moreover, the increasing phase angle of nearly 90° confirms the frequency dispersion has increased the iron's protection and LS inhibitor adsorption.

Table 1

Electrochemical impedance parameters of mild steel in 1M HCl

Conc (ppm)	Temp (°C)	R_{inh} (Ωcm^2)	R_{ct} (Ω cm^2)	Y_o (×10^{-6} Ω^{-1} cm^{-2} S^n)	n	Corr Rate (mmpy)	Efficiency (%)
Blank	30	4.87	0.7913	0.001199	0.8816	512.7	0
Blank	40	2.576	0.7268	0.001949	0.9007	760.7	0
Blank	50	1.431	0.679	0.003363	0.8867	1186	0
20	30	29.94	1.115	0.003403	0.6036	33.14	83.73
20	40	66.97	0.9222	0.000461	0.7662	35.96	96.15
20	50	39.67	0.8841	0.000415	0.7902	44.77	96.39
40	30	63.16	0.008545	0.00002	0.3496	86.37	92.28
40	40	18.32	0.8274	0.000631	0.8111	71.4	85.93
40	50	7.971	0.7719	0.000923	0.7842	243.1	82.04
60	30	108.9	1.689	0.00052	0.7395	15.36	95.52
60	40	29.09	1.314	0.000624	0.7377	201.2	91.14
60	50	15.41	1.311	0.001047	0.711	690.5	90.71
80	30	243.7	10.08	0.000333	0.7576	13.81	98.00
80	40	264.8	9.404	0.000319	0.7378	23.62	99.02
80	50	834.9	0.02845	0.000329	0.7396	29.32	99.82

5. 1. 2. The bioactive of Liquid Smoke inhibitor characterization results

Gas Chromatography-Mass Spectroscopy (GC-MS) results show detailed knowledge about the bioactive compound of the inhibitor, as presented in Table 2.

Similar to the work [29], the LS inhibitor is characterized using GC-MS and is presented in Table 2. It is concluded that the pyrolysis condensation process constitutes various natural compounds with different chemical compositions and retention times. The primary mixture of LS is the phenolic molecules, which have become the dominant compound in RHA extract. Similar work shows that the compound of 2-((thiazole-2-ylimino) methyl) phenol [30] adsorbs on mild steel, reduces the number of pit corrosion, and modifies the surface of damaged steel due to corro-

sion. Moreover, Cyclononasiloxane, octadecamethyl, and Tetracosamethyl-cyclododecasiloxane exhibit the longest retention time of 177.992 and 251.971 seconds to suggest the general characteristic of LS inhibitors fits the requirement for green corrosion inhibitor.

Table 2

The major bioactive component LS inhibitor

Chemical Compounds	Retention Time (s)	Qual number
Phenol, 2-methyl-	82.965	97
p-Cresol	86.493	96
Phenol, 2,6-dimethyl-	91.913	96
Phenol, 2,4-dimethyl-	98.088	96
Phenol	71.118	95
Phenol, 4-ethyl-	100.987	95
2-Furancarboxaldehyde, 5-methyl-	69.227	94
Phenol, 3,5-dimethyl-	102.499	94
Pyridine, 2-methyl-	45.282	93
Phenol, 2-methoxy-	88.636	93
Cyclononasiloxane, octadecamethyl-	177.992	93
2-Cyclopenten-1-one	47.172	91
2-Cyclopenten-1-one, 2-methyl-	58.893	91
Phenol, 3-methyl-	89.896	91
Tetracosamethyl-cyclododecasiloxane	251.971	91
Cyclodecasiloxane, eicosamethyl-	193.115	90
2-Cyclopenten-1-one	4.881	87
2-Cyclopenten-1-one, 2,3-dimethyl-	81.074	87
2-Methoxy-5-methylphenol	104.768	87
2-Cyclopenten-1-one, 3,4-dimethyl-	73.764	86
Furan, 2-ethyl-	52.969	81
Tetracosamethyl-cyclododecasiloxane	241.763	81

5. 2. The result of actual functional groups characterization results

As previously outlined, the primary bioactive compound of LS shows its capability to protect the substrate. In this work, the Raman Spectroscopy spectrum is utilized to examine the structure of accumulated adsorption inhibitors of the pre and post-film formation. The spectra are illustrated in Fig. 3.

Overall, the weak band at 458 cm^{-1} corresponds to the presence of silanol functional group (Si–OH) and siloxane (Si–O–Si) [31], which predicts binding with reduced iron ions. This fact agrees with [32] to unveil the reduction of the δ–FeOOH phase within the range of 420 and 663 cm^{-1}. The spectra at 662 cm^{-1} attributed to the presence of Fe_3O_4 confirmed by [33], and also it shows highly mixed in C–C complex molecules, as previously published by [25]. The peak at about 860 cm^{-1} may be associated with an aromatic ring functional group of phenol, 2,4-dimethyl- which leads to a dative covalent bond formation. Bands between 1095-1100 cm^{-1} were correlated to asymmetric C–O–C and confirmed the presence of cellulose in the passive film of inhibited steel [34]. The aromatic ring of phenol, 3,5-dimethyl- spectra at 1095 cm^{-1} amplifies this observation due to a considerably longer retention time molecular weight. The highest peak at around 1350 cm^{-1} corresponds to cyclononasiloxane, octadecamethyl and tetracosamethyl-cyclododecasiloxane and its respective adsorption functional groups molecule of CH_3–Si–O– on the substrate.

The author of [35] verifies the high solubility of tetracosamethyl-cyclododecasiloxane (R–COO–R', an ester functional group) in water and enriches the LS inhibitor's "green" concept to reduce the adverse environmental effect upon inhibitor disposal. The identified peak of oxygen-free functional groups at 1450 and 1595 cm^{-1} attributes with CH_3–CH_2 deformation and >CH_2 at 2880 cm^{-1}. Meanwhile, the >C=O (carbonyl) functional group correlates to the appearance peak at 1780 cm^{-1} (Table 2). After the adsorption of the inhibitor, the dramatic change in the peak height at 3240 cm^{-1} correlates to aromatic –CH derivatives molecules and the broadened peak due to hydrogen bonding. A similar result confirms the interaction of polarized molecules in 2-Furancarboxaldehyde, 5-methyl and Furan, 2-ethyl- and the iron ions [36]. Eventually, the sharp decrease of the peak at 3530 cm^{-1} demonstrates the wider surface coverage area of protection through intense adsorption of the –OH functional group [37].

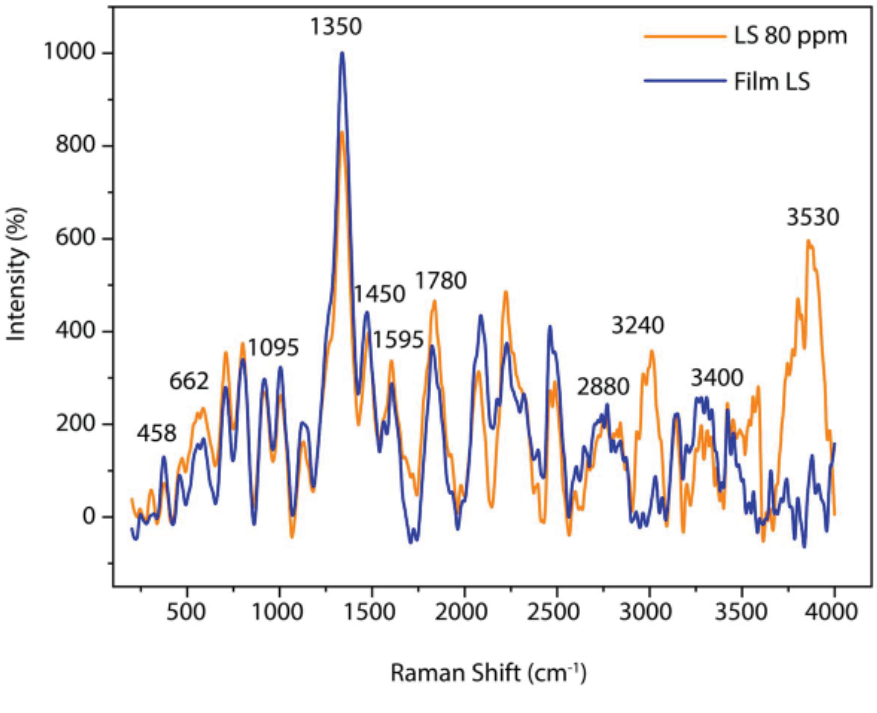

Fig. 3. The Raman Spectrum of Adsorption Model

5. 3. The nature of inhibitor adsorption results

Table 3 shows the thermodynamic parameters result of the electrochemical measurements at various concentrations and temperatures.

Table 3

The thermodynamic inhibitor parameter and its surface coverage

Conc (ppm)	Temp (°C)	K_{ads} (L mol^{-1})	ΔG_{ads} (kJ/mol)	ΔH_{ads} (kJ/mol)	ΔS_{ads} (kJ/mol)	Surface Coverage (θ)
20	303	0.1715	4.4402	15.5514	36.6704	0.8373
20	313	0.6249	1.2233	16.0646	48.9813	0.9615
20	323	0.5344	1.6825	16.5779	49.1597	0.9639
40	303	0.3989	2.3147	15.5514	43.6854	0.9228
40	313	0.1527	4.8887	16.0646	36.8840	0.8593
40	323	0.0914	6.4247	16.5779	33.5087	0.8204
60	303	0.7120	0.8555	15.5514	48.5012	0.9552
60	313	0.2573	3.5324	16.0646	41.3604	0.9114
60	323	0.1953	4.3848	16.5779	40.2410	0.9071
80	303	1.6347	–1.2380	15.5514	55.4108	0.9800
80	313	2.5448	–2.4307	16.0646	61.0409	0.9902
80	323	11.6487	–6.5932	16.5779	76.4724	0.9982

The evolution of passive film correlates to the value of adsorption and desorption constant, K_{ads} (Table 2). At lower concentration (20 ppm) and high temperature (323 K), the value of K_{ads} is 0.534437, which is relatively more significant than the 40 and 60 ppm at the same temperature. Raising the concentration (80 ppm) increases the stability of adsorbed film at 11.648 L mol^{-1} despite a slight deviation occurring. It shows that the strength of the inhibitor's film may correspond to the adsorption's effectiveness of the LS inhibitor on the steel's surface.

(2) shows the relationship between the free energy Gibbs (ΔG_{ads}) and the value of $K_{ads,}$ and the value attributes to the adsorption classification of LS.

$$\left\{\Delta G_{ads} = -RT\ln\left(1\times10^{6}K_{ads}\right)\right\}. \quad (2)$$

In the above equation, R is the ideal gas constant (8.314 J/K moles), and T is the absolute temperature (K). The literature states that the physisorption ranges from –20 kJ/mol or less, confirming the polar interaction between the inhibitor and positively charged iron atom [38]. On the contrary, the value of ΔG_{ads} greater than –40 kJ/mol or more negative indicates the formation of a coordinate bond through chemisorption [39]. The information on adsorption isotherm applies to confirm the chemisorption behavior of LS inhibitors. The plotting between C/θ versus $1/K_{ads}$ provides the value of R^2, as calculated using (3) [40].

The plotting between C/θ versus $1/K_{ads}$ provides the value of $R^{2,}$ as calculated using (3) [40].

$$\left\{\frac{C}{\theta} = \frac{1}{K_{ads}} + C\right\}. \quad (3)$$

In the above equation, C is the concentration of inhibitor (mol/dm^3), θ is the surface coverage area, and K_{ads} is the adsorption/desorption constant (mol·L^{-1}). According to the calculation, the linear regression coefficient of R^2 shows the adsorption of LS is in good agreement with Langmuir adsorption, which provided the value of R^2 of 0.9079. It remains significant to remember the maximum value of K_{ads} of 11.64876 occurs at 80 ppm (323 K).

5. 4. Surface Treatment Morphology Analysis results

5. 4. 1. Scanning Electronic Microscope and Energy-Dispersive X-Ray Spectroscopy results

Fig. 4 shows the SEM image of the mild steel surface before and after adding the inhibitor for 1 hour.

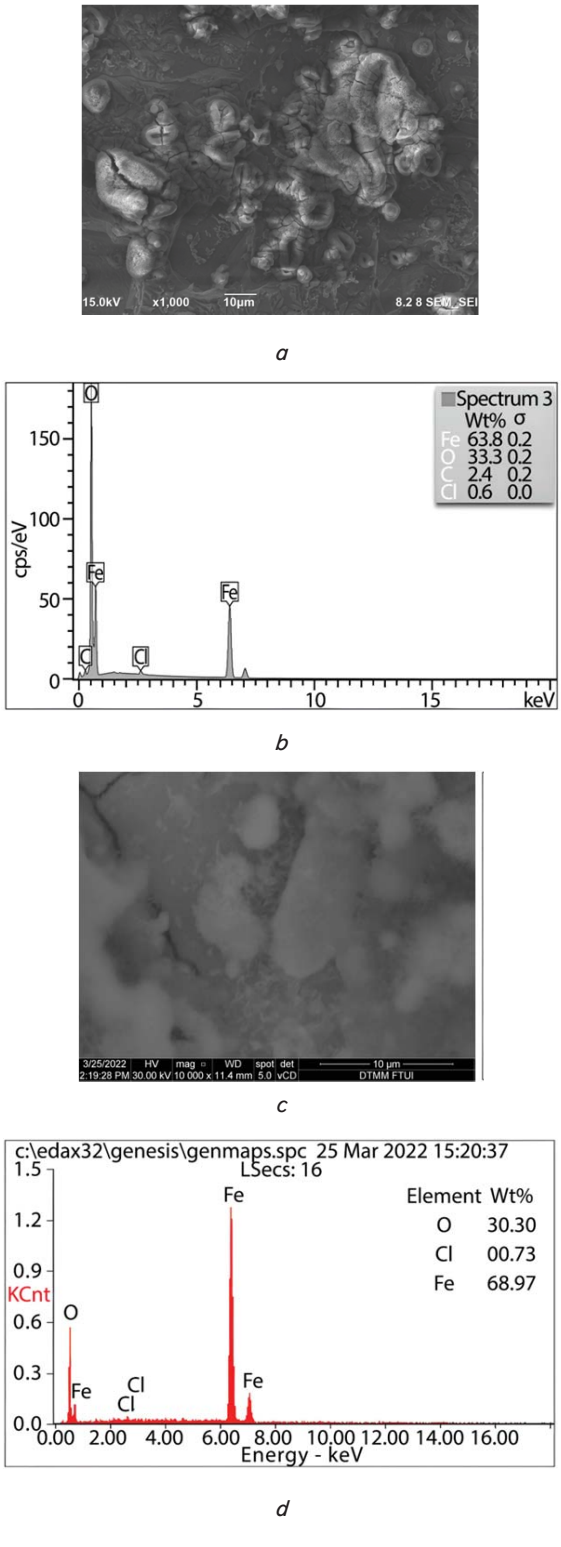

Fig. 4. Surface Treatment results of: *a, b* — uninhibited; *c, d* — inhibited mild steel

It can be seen that before the introduction of the inhibitor, the surface of the steel was severely damaged. It shows the increase of surface roughness due to the significant intensified metals' dissolution (Fig. 4). The corrosion products of $Fe(OH)_2$ and $Fe(OH)_3$ appear after immersion without inhibitors. On the contrary, the highest amount of iron was identified on the substrate of MS in 80 ppm inhibitor (68.97 %), confirming inhibitor molecules' adsorption and increasing the surface coverage area, as shown in Table 2. The unprotected metal has high chloride and oxygen content of 0.6 % and 33.3 %. On the contrary, the inhibited metal shows depression of the same elements at 0.73 % and 30.3 %, which provides the adsorption process has increased the evolution of the passive film thickness layer.

5. 4. 2. Atomic Force Microscopy and Contact Angle results

The AFM figures and their corresponding two-dimensional texture heights provide the surface morphology of the substrate before and after the addition of inhibitor (Fig. 5).

Fig. 5, *a, c* compare the observable changes in the mild steel surface, which are indicated by the less peak and an increasing number of the valley. The surface post the addition of inhibitor is smoother and confirms the result in Fig. 4, *b*. According to [41], the lower skewness value corresponds to the minor peak and proves the adsorption process. Upon addition of an inhibitor, the skewness values in uninhibited steel are –0.2189 and continuously decrease to –0.1293. The fact is also related to the declining value of maximum roughness peak height (R_p) from 1.215 nm to 0.2760 nm. The root-mean-square roughness (R_q) difference of 0.3824 nm shows the surface modification and its inhibition effect.

The inhibition of the LS correlates to the increase in the hydrophobic surface of the metal. Fig. 6 shows the two contact angle measurements for mild steel in the HCl 1M solution comprising various concentrations of LS inhibitor 0 and 80 ppm.

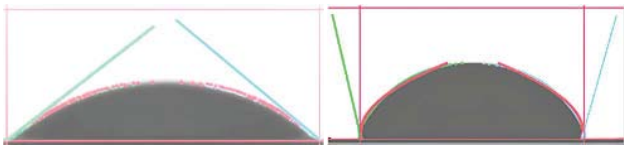

a *b*

Fig. 6. The contact angle measurements: *a* — Blank solution; *b* – 80 ppm inhibitor solution

According to Fig. 6, *a*, the surface of mild steel has a low contact angle of 38.94°, which corresponds to the lower substrate hydrophilicity. In addition to 80 ppm solution, the contact angle increases to 104.41°, unveilings that the adsorption of LS inhibitor reduces the wettability of the substrate's surface.

6. Discussion of the Liquid Smoke as green corrosion inhibitors

The scope of this research results includes the discussion of the anticorrosion of inhibitors, the identification of primary compounds in the liquid smoke, the determination of adsorbed functional groups on the surface of metals, the thermodynamic of the adsorption process, and the effect of the inhibitor on the surface treatment of the severe mild steel.

The Potentiodynamic Polarization (PP) test shows similar trends in the cathodic and anodic regions to provide information on a similar inhibition mechanism. In the cathodic area, the inhibitor lowers the evolution of hydrogen gas, while the attachment of the inhibitor to the anodic region reduces the likelihood of electron's dismissal. The potential corrosion, E_{corr}, increases attributed to the passive layer condensation to reduce mild steel's general (pitting) corrosion [42]. However, the movement of potential corrosion in the anodic region provides clear evidence related to the weak electrostatic interactions between the negative dipole of inhibitor and the positive dipole of metals (Fe^{2+} or Fe^{3+}). On the other hand, the lower corrosion density at higher concentrations can be correlated to the increasing protective multilayer of inhibitors on the surface of mild steel. It also relates to decreasing metal dissolved in HCl 1M [43–45].

The result of PP agrees well with the outcome of the EIS test. The EIS method is suitable for demonstrating the information related to the reaction of the metal/electrolyte interface and its corrosion activities. Notably, the increased concentration of LS inhibitor molecules correlates to the increasing charge transfer

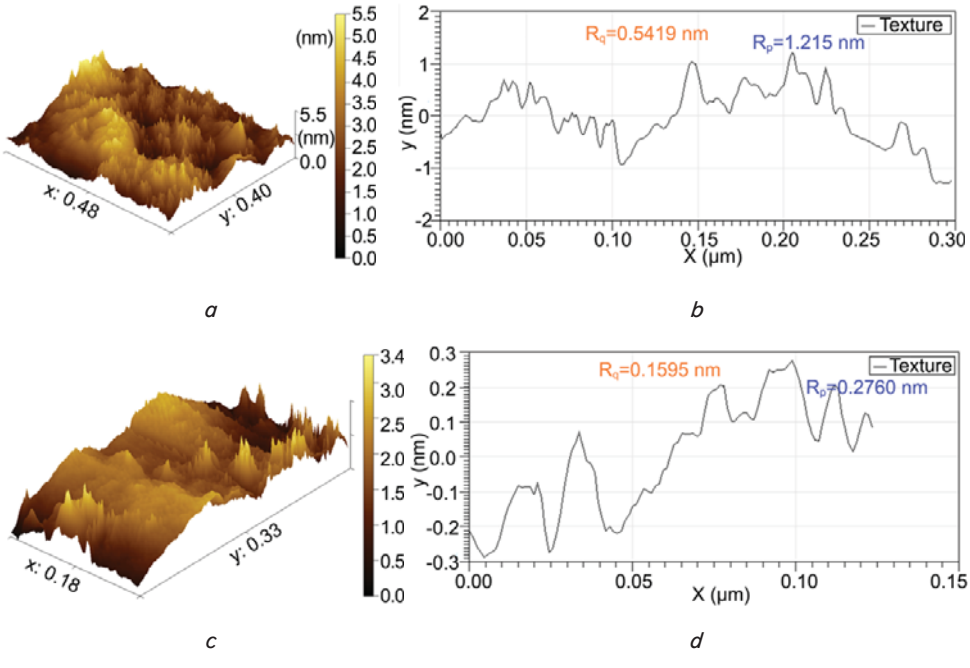

a *b* *c* *d*

Fig. 5. The Atomic Force Microscopy 3D topography result and 2D Height Plots: *a, b* – Uninhibited Mild Steel; *c, d* – Inhibited at 80 ppm solution

resistance (Fig. 1, *b*). It includes the process of mass transfer, surface roughness, and increasing electrode inhomogeneity. As shown in the same figure, the shape of the semicircle of the one-time constant graph remains constant, indicating the inhibitors work at the exact inhibition mechanism of mild steel in a hydrochloric acid medium [46]. It can be seen that the entire plots show a similar shape due to elongation of the capacitive loops in increasing concentration. The similar shape indicates the related corrosion inhibition mechanism due to the charge transfer process from the LS inhibitor to the substrate, except in the blank solution.

On the contrary, at 80 ppm, the LS inhibitor demonstrates its capability to form a passive layer and reduce the penetration of chloride ions and molecules of water. The phenomenon is associated with a longer Nyquist diameter at nearly 150 Ω cm^2, generally observed from the considerable inhibitor (charge transfer resistance) value in Table 1. In addition, the appearance of a single capacitive loop represents the dispersion of frequency measurement due to LS inhibitor reduces the mass transfer and dismissal of the electron [47] in high concentrated inhibitor's medium. The frequency dispersion demonstrates the adsorption of LS inhibitors and increases the surface heterogeneity, similar to the published work of [48].

Given the significant inhibition effect of LS, the combination of a large amount of phenol-2-methyl-, pyridine, 2-methyl-Cyclononasiloxane, and octadecamethyl are sufficient to form the protonated ionic molecules. The superior efficiency inhibition (IE) of about 99 % corresponds with the adsorbed these molecules. At higher IE, the LS inhibitor weakens the corrosion degree of mild steel, as shown by increasing semicircle diameter. As observed in Fig. 1, *b*, a remarkable change in Nyquist diameter is in good agreement with the result of the Bode Plot and Phase. The phase angle of the inhibited solution is wider than unprotected mild steel (Fig. 1, *d*), proving the more adsorbed bioactive molecules of RHA. The same pattern was observed in the Bode Plot graph at various concentrations. At low frequency, the value of log *Z* increases, indicating that a higher inhibitor dose in the interface between the mild steel and LS solution shows a typical ideal capacitor [28]. This result agrees with the observable one-time constant of the Bode plot and correlates to the presence of an electric double layer. Moreover, the increasing phase angle of nearly 90° confirms the frequency dispersion has increased the iron's protection and LS inhibitor adsorption.

Unlike the common trend of inhibitors, the Electrochemical measurements show that a lower concentration of 20 ppm has a higher Nyquist diameter, impedance, and phase angle (Fig. 1, *b–d*) than 40 and 60 ppm. Similarly, the solution's corrosion rate and inhibition efficiency above give an irregular trend (Table 1). At 20 ppm, the inhibition efficiency stands at 96.39 %, dropping slightly to 82.04 % at 40 ppm solution. The primary reason for anticorrosion's reduction can be judged by the vertical adsorption of LS inhibitor on the surface of a metallic atom, which is the opposite of the parallel direction model of an inhibitor to achieve optimum surface coverage [49]. Therefore, all of these conditions elucidate that LS has better inhibition performance increases from 20 ppm to 80 ppm and fitted the Electrical Equivalent circuit (Fig. 2). As shown in Table 1 and Fig. 2, the CPE of the solution comprises the passivity (Y_0) and capacitance or resistance of the solution (*n*). Before adding an inhibitor, the value of Y_0 and *n* is higher than 0.003363 and 0.8867 and continuously decreases to 0.000329 and 0.7396. The decrease in these values indicates more water molecules are being replaced by LS molecules as the local dielectric constant decrease and rises the thickness of the capacitor [50]. The contributor to the depression of CPE corresponds with the adsorption of the protonated molecules, which comprise heterocyclic rings and oxygenated functional groups adsorbed on the steel [51] (Table 1). Hence, these active compounds show the inhibitor's stability and strength through physical adsorption and extending metal protection from corrodents.

The Raman Spectroscopy result confirms the interaction of these bioactive molecules with the substrate by showing multiple peaks related to the adsorption process. As shown in Table 2, the silanol functional group can bind with the iron ions. The work of [52] shows that the network of Si–O–Si gives a better barrier to protect the metal from corrosion. At the same time, the peak around 400 to 650 cm^{-1} corresponds to the reduction of δ–FeOOH to slow the oxidation process reported by [53]. Furthermore, the presence of Fe_3O_4 shows that the inhibitor retains the Fe^{3+} ions and reduces the possible reduction to Fe^{2+} ions. The aromatic ring peaks at 860 $cm^{-1,}$ demonstrating the capability of the inhibitor to form a passive film and enlarging the surface coverage area protection [54]. The contribution of a phenolic compound of LS towards the inhibition process correlates to the increasing layers of the passive film [55].

All these results align with the LS inhibitor's chemisorption as more electrons are transferred or shared between the adsorbate and the mild steel. It results from the dative-covalent bond in which the interaction is stronger than physisorption. During the bond formation, the complex of Fe-LS inhibitor is given where the LS inhibitors molecules play a part in the bond breaking and forming process on the surface of mild steel. This work shows four major organic molecules in LS of phenolic, Pyridine, Cyclononasiloxane, octadecamethyl to overlap their orbital to the 3d atomic orbital of Fe to result in the new bonding and becomes critical when mild steel is exposed in HCl 1M. In this case, the molecules behave as a ligand to form a Fe-ligand complex compound supported by the value of ΔG_{ads}.

Furthermore, the value of ΔH_{ads} of 16.5 kJ/mol shows inhibitor adsorption is quicker at higher temperatures, with more energy required to solidify the liquid LS inhibitor. The finding agrees well with the immense entropy value and corresponds with the high affinity of the inhibitor to the surface of the metal [56]. Hence, it may be indicated that the inhibitor is formed a monolayer passive film on mild steel, which is confirmed by the result of isotherm adsorption of Langmuir. The nearness value of R^2 to 1 (0.9079) shows the equivalency between the adsorption and desorption rates and the high value of K_{ads}. In this case, the value assumes that all sites of corroded area (due to pitting corrosion) have the same affinity towards the LS inhibitors, and the number of adsorbed molecules is limitless [57]. As a result, a more inhibited area is observed, as shown in Fig. 4, *b*. On the inhibited substrate, the result of EDX shows a significant reduction of chloride ions and a regaining amount of iron atoms. Despite only a slight change of oxygen atom identified, it can be concluded the adsorption of LS triggers the multisite adsorption of Langmuir (Fig. 4, *b*). The multiple adsorption sites prove that numerous elementary adsorption sites are located on the metallic surface where one site fits for their corresponding single adsorbed LS molecules [58].

The result of SEM and EDX aligns with the remarkable reduction of AFM surface roughness and increasing contact

angle between the inhibitor and mild steel. In the preceding section, the skewness value dramatically decreased, corresponding to the surface treatment and a smoother surface. It was found that the root-mean-square roughness (R_q) is reduced to support the evidence of increasing hydrophobicity of inhibitors. The result shows that the hydrophobic agglomerate passive film with phenolic, pyridine, and Cyclononasiloxane groups on its surface is considered a small inhibitor molecule to remove more water molecules by forming a hydrophobic barrier.

The limitation of this research is correlated to the types of characterization of inhibitors on the mild steel under HCl 1M solution. For instance, SEM-EDX in this work to study the evolution of film thickness as a more concentrated inhibitor was added. It disadvantages the research concerning determining the depth of pitting corrosion that has influenced metals' mechanical properties depletion. Furthermore, it also impacts the investigation of the pitting corrosion potential and re-passivation potential related to forming a film barrier between the substrate and solution.

The possible development to address the restriction in the preceding phenomenon is by giving intensive attention to the corroded materials' potential re-passivation and corrosion pitting potential. However, the possible difficulty might be related to how the calculated value gives a better explanation to comprehend the relationship between the evolution thickness of the passive film and the higher impedance. It is also noteworthy to remember that the thicker size of the film corresponds to the protection of metal and lowers the pitting corrosion potential of metal. It also shifts the re-passivation potential to a more negative corrosion potential and causes the metal to be protected.

Overall, the expected result of the above research can be implemented in pipeline protection. The high value of the adsorption-desorption constant of K_{ads} shows that the inhibitor is attracted to promote immense surface protection of 0.9982. Moreover, SEM-EDX results show that most of the corrosion pit is recovered to achieve maximum protection. The AFM result shows the average surface roughness is dramatically decreased, which aligned with the increase of hydrophobicity of the substrate at 104.41°. The research could be a provision to increase the integrity of pipelines due to high efficiency and lower toxicity upon disposal in the marine system using rice husks ashs at affordable cost.

7. Conclusions

1. Unveiling the potential of LS as a green corrosion inhibitor shows that the phenolic, pyridine, cyclononasiloxane, and octadecamethyl are primary bioactive molecules of RHA to inhibit the corrosion rate of the mild steel under HCl 1M solution. The adsorption of the molecules provides superior inhibition efficiency. It shows the rapid increase of Nyquist semicircle diameter, high Bode phase angles, and a higher impedance value.

2. The adsorption of the above molecules is reflected in the Raman spectroscopy results, where the absorption of aromatic rings, –OH, C–O–C, C=O, Si–O–Si, are identified. The corresponding functional group is adsorbed to prove the inhibition reaction has occurred.

3. The thermodynamic calculation shows the formation of dative covalent bonding (chemisorption) where monolayer film formation is observed at higher temperature and concentrations. It confirms the Langmuir isothermic adsorption process and increases the surface coverage area of protection.

4. The result of SEM-EDX confirms the deposition of monolayer film to reduce the number of corrosion pit and increase the composition of iron and oxygen. At the same time, it lowers the number of chloride ions, as shown by the result of EDX on the inhibited surface. The AFM and Contact angle measurements agree well with the SEM-EDX, where the reduction in skewness value is identified and increases the hydrophobicity of metal towards polar molecules of water and HCl 1M.

Conflict of interest

The authors declare that they have no conflict of interest in relation to this research, whether financial, personal, authorship or otherwise, that could affect the research and its results presented in this paper.

Acknowledgment

The author gratefully thanks the Ministry of Research and Technology/National Research and Innovation Agency for the financial support of contract number NKB-1008/UN2.RST/HKP.05.00/2022.

References

1. Guillal, A., Ben Seghier, M. E. A., Nourddine, A., Correia, J. A. F. O., Bt Mustaffa, Z., Trung, N.-T. (2020). Probabilistic investigation on the reliability assessment of mid- and high-strength pipelines under corrosion and fracture conditions. Engineering Failure Analysis, 118, 104891. doi: https://doi.org/10.1016/j.engfailanal.2020.104891
2. Simmons, M. R. (2008). Report of offshore technology conference (OTC) presentation. Houston, TX: NACE International Oil and Gas Production.
3. Gupta, N. K., Verma, C., Salghi, R., Lgaz, H., Mukherjee, A. K., Quraishi, M. A. (2017). New phosphonate based corrosion inhibitors for mild steel in hydrochloric acid useful for industrial pickling processes: experimental and theoretical approach. New Journal of Chemistry, 41 (21), 13114–13129. doi: https://doi.org/10.1039/c7nj01431g
4. Aditiyawarman, T., Kaban, A. P. S., Soedarsono, J. W. (2022). A Recent Review of Risk-Based Inspection Development to Support Service Excellence in the Oil and Gas Industry: An Artificial Intelligence Perspective. ASCE-ASME J Risk and Uncert in Engrg Sys Part B Mech Engrg, 9 (1). doi: https://doi.org/10.1115/1.4054558
5. Aditiyawarman, T., Soedarsono, J. W., Kaban, A. P. S., Riastuti, R., Rahmadani, H. (2022). The Study of Artificial Intelligent in Risk-Based Inspection Assessment and Screening: A Study Case of Inline Inspection. ASCE-ASME Journal of Risk and Uncertainty in Engineering Systems, Part B: Mechanical Engineering, 9 (1). doi: https://doi.org/10.1115/1.4054969

6. Pumps, S. (2010). Materials and Corrosion. Centrifugal Pump Handbook, 227–250. doi: https://doi.org/10.1016/b978-0-7506-8612-9.00008-5
7. Wasim, M., Djukic, M. B. (2021). Corrosion induced failure of the ductile iron pipes at micro- and nano-levels. Engineering Failure Analysis, 121, 105169. doi: https://doi.org/10.1016/j.engfailanal.2020.105169
8. Jawad, M. N., Amouzad Mahdiraji, G., Hajibeigy, M. T. (2020). Performance improvement of sacrificial anode cathodic protection system for above ground storage tank. SN Applied Sciences, 2 (12). doi: https://doi.org/10.1007/s42452-020-03823-7
9. Baloyi, T., Maledi, N., Andrews, A. (2022). Corrosion performance of zinc phosphate coatings deposited on AA6061-HDG steel. Materials Chemistry and Physics, 283, 126009. doi: https://doi.org/10.1016/j.matchemphys.2022.126009
10. Fløe, N. E., Faramarzi, L., Iversen, F., Kleppe, E. R., Graver, B., Bryntesen, H. N., Johnsen, K. (2019). Assessment of material selection for the CO2 absorption process with aqueous MEA solution based on results from corrosion monitoring at Technology Centre Mongstad. International Journal of Greenhouse Gas Control, 84, 91–110. doi: https://doi.org/10.1016/j.ijggc.2019.02.004
11. Kaban, A. P. S., Ridhova, A., Priyotomo, G., Elya, B., Maksum, A., Sadeli, Y. et. al. (2021). Development of white tea extract as green corrosion inhibitor in mild steel under 1 M hydrochloric acid solution. Eastern-European Journal of Enterprise Technologies, 2 (6 (110)), 6–20. doi: https://doi.org/10.15587/1729-4061.2021.224435
12. Arlan, A. S., Subekti, N., Soedarsono, J. W., Rustandi, A. (2018). Corrosion Inhibition by a Caesalpinia Sappan L Modified Imidazoline for Carbon Steel API 5L Grade X60 in HCl 1M Environment. Materials Science Forum, 929, 158–170. doi: https://doi.org/10.4028/www.scientific.net/msf.929.158
13. Soedarsono, J. W., Shihab, M. N., Azmi, M. F., Maksum, A. (2018). Study of curcuma xanthorrhiza extract as green inhibitor for API 5L X42 steel in 1M HCl solution. IOP Conference Series: Earth and Environmental Science, 105, 012060. doi: https://doi.org/10.1088/1755-1315/105/1/012060
14. Kadhim, A., Al-Amiery, A. A., Alazawi, R., Al-Ghezi, M. K. S., Abass, R. H. (2021). Corrosion inhibitors. A review. International Journal of Corrosion and Scale Inhibition, 10 (1). doi: https://doi.org/10.17675/2305-6894-2021-10-1-3
15. Lin, B., Shao, J., Xu, Y., Lai, Y., Zhao, Z. (2021). Adsorption and corrosion of renewable inhibitor of Pomelo peel extract for mild steel in phosphoric acid solution. Arabian Journal of Chemistry, 14 (5), 103114. doi: https://doi.org/10.1016/j.arabjc.2021.103114
16. Verma, C., Quraishi, M. A., Rhee, K. Y. (2021). Present and emerging trends in using pharmaceutically active compounds as aqueous phase corrosion inhibitors. Journal of Molecular Liquids, 328, 115395. doi: https://doi.org/10.1016/j.molliq.2021.115395
17. Rustandi, A., Soedarsono, J. W., Suharno, B. (2011). The Use of Mixture of Piper Betle and Green Tea as a Green Corrosion Inhibitor for API X-52 Steel in Aerated 3.5 % NaCl Solution at Various Rotation Rates. Advanced Materials Research, 383-390, 5418–5425. doi: https://doi.org/10.4028/www.scientific.net/amr.383-390.5418
18. Azmi, M. F., Soedarsono, J. W. (2018). Study of corrosion resistrance of pipeline API 5L X42 using green inhibitor bawang dayak (Eleutherine americanna Merr.) in 1M HCl. IOP Conference Series: Earth and Environmental Science, 105, 012061. doi: https://doi.org/10.1088/1755-1315/105/1/012061
19. Kaban, E. E., Maksum, A., Permana, S., Soedarsono, J. W. (2018). Utilization of secang heartwood (caesalpinia sappan l) as a green corrosion inhibitor on carbon steel (API 5L Gr. B) in 3.5% NaCl environment. IOP Conference Series: Earth and Environmental Science, 105, 012062. doi: https://doi.org/10.1088/1755-1315/105/1/012062
20. Kusumastuti, R., Pramana, R. I., Soedarsono, J. W. (2017). The use of morinda citrifolia as a green corrosion inhibitor for low carbon steel in 3.5% NaCl solution. AIP Conference Proceedings. doi: https://doi.org/10.1063/1.4978085
21. Soltani, N., Bahrami, A., Pech-Canul, M. I., González, L. A. (2015). Review on the physicochemical treatments of rice husk for production of advanced materials. Chemical Engineering Journal, 264, 899–935. doi: https://doi.org/10.1016/j.cej.2014.11.056
22. Daniel-Mkpume, C. C., Aigbodion, V. S., Obikwelu, D. O. N. (2021). Electrochemical analysis and microstructure of value-added functional Zn-ZnO-rice husk ash composite coating of mild steel. Chemical Data Collections, 35, 100767. doi: https://doi.org/10.1016/j.cdc.2021.100767
23. Nisar, N., Bhat, J. A. (2020). Experimental investigation of Rice Husk Ash on compressive strength, carbonation and corrosion resistance of reinforced concrete. Australian Journal of Civil Engineering, 19 (2), 155–163. doi: https://doi.org/10.1080/14488353.2020.1838419
24. Awizar, D. A., Othman, N. K., Jalar, A., Daud, A. R., Rahman, I. A., Al-Hardan, N. H. (2013). Nanosilicate extraction from rice husk ash as green corrosion inhibitor. International Journal of Electrochemical Science, 8, 1759–1769. Available at: https://citeseerx.ist.psu.edu/viewdoc/download?doi=10.1.1.654.1036&rep=rep1&type=pdf
25. Paul Setiawan Kaban, A., Mayangsari, W., Syaiful Anwar, M., Maksum, A., Riastuti, R., Aditiyawarman, T., Wahyuadi Soedarsono, J. (2022). Experimental and modelling waste rice husk ash as a novel green corrosion inhibitor under acidic environment. Materials Today: Proceedings, 62, 4225–4234. doi: https://doi.org/10.1016/j.matpr.2022.04.738
26. King, A. D., Birbilis, N., Scully, J. R. (2014). Accurate Electrochemical Measurement of Magnesium Corrosion Rates; a Combined Impedance, Mass-Loss and Hydrogen Collection Study. Electrochimica Acta, 121, 394–406. doi: https://doi.org/10.1016/j.electacta.2013.12.124
27. Zhao, Q., Guo, J., Cui, G., Han, T., Wu, Y. (2020). Chitosan derivatives as green corrosion inhibitors for P110 steel in a carbon dioxide environment. Colloids and Surfaces B: Biointerfaces, 194, 111150. doi: https://doi.org/10.1016/j.colsurfb.2020.111150
28. Ansari, K. R., Quraishi, M. A., Singh, A. (2015). Isatin derivatives as a non-toxic corrosion inhibitor for mild steel in 20% H_2SO_4. Corrosion Science, 95, 62–70. doi: https://doi.org/10.1016/j.corsci.2015.02.010

29. Khadraoui, A., Khelifa, A., Hadjmeliani, M., Mehdaoui, R., Hachama, K., Tidu, A. et. al. (2016). Extraction, characterization and anti-corrosion activity of Mentha pulegium oil: Weight loss, electrochemical, thermodynamic and surface studies. Journal of Molecular Liquids, 216, 724–731. doi: https://doi.org/10.1016/j.molliq.2016.02.005
30. Yilmaz, N., Fitoz, A., Ergun, U., Emregül, K. C. (2016). A combined electrochemical and theoretical study into the effect of 2-((thiazole-2-ylimino)methyl)phenol as a corrosion inhibitor for mild steel in a highly acidic environment. Corrosion Science, 111, 110–120. doi: https://doi.org/10.1016/j.corsci.2016.05.002
31. Pereira, M. A., Oliveira, J. E. de, Fonseca, C. S. (2021). Influence of the use of rice husk as source of silica on the sol-gel synthesis of bioglass. Cerâmica, 67 (383), 333–337. doi: https://doi.org/10.1590/0366-69132021673833134
32. Bergmann CP, P. P. (2015). Raman Spectroscopy of Iron Oxide of Nanoparticles (Fe_3O4). Journal of Material Science & Engineering, 05 (01). doi: https://doi.org/10.4172/2169-0022.1000217
33. Hanesch, M. (2009). Raman spectroscopy of iron oxides and (oxy)hydroxides at low laser power and possible applications in environmental magnetic studies. Geophysical Journal International, 177 (3), 941–948. doi: https://doi.org/10.1111/j.1365-246x.2009.04122.x
34. Yu, Y., Ramachandran, P. V., Wang, M. C. (2014). Shedding new light on lipid functions with CARS and SRS microscopy. Biochimica et Biophysica Acta (BBA) - Molecular and Cell Biology of Lipids, 1841 (8), 1120–1129. doi: https://doi.org/10.1016/j.bbalip.2014.02.003
35. Gupta, A., Kumar, M., Ghosh, P., Swati, Thakur, I. S. (2022). Risk assessment of a municipal extended aeration activated sludge treatment plant using physico-chemical and in vitro bioassay analyses. Environmental Technology & Innovation, 26, 102254. doi: https://doi.org/10.1016/j.eti.2021.102254
36. Akalezi, C. O., Maduabuchi, A. C., Enenebeaku, C. K., Oguzie, E. E. (2020). Experimental and DFT evaluation of adsorption and inhibitive properties of Moringa oliefera extract on mild steel corrosion in acidic media. Arabian Journal of Chemistry, 13 (12), 9270–9282. doi: https://doi.org/10.1016/j.arabjc.2020.11.010
37. Li, S., Qi, B., Luo, J., Zhuang, Y., Wan, Y. (2021). Ultrafast selective adsorption of pretreatment inhibitors from lignocellulosic hydrolysate with metal-organic frameworks: Performance and adsorption mechanisms. Separation and Purification Technology, 275, 119183. doi: https://doi.org/10.1016/j.seppur.2021.119183
38. Chelliah, N. M., Padaikathan, P., Kumar, R. (2019). Evaluation of electrochemical impedance and biocorrosion characteristics of as-cast and T4 heat treated AZ91 Mg-alloys in Ringer's solution. Journal of Magnesium and Alloys, 7 (1), 134–143. doi: https://doi.org/10.1016/j.jma.2019.01.005
39. Verma, C., Olasunkanmi, L. O., Ebenso, E. E., Quraishi, M. A., Obot, I. B. (2016). Adsorption Behavior of Glucosamine-Based, Pyrimidine-Fused Heterocycles as Green Corrosion Inhibitors for Mild Steel: Experimental and Theoretical Studies. The Journal of Physical Chemistry C, 120 (21), 11598–11611. doi: https://doi.org/10.1021/acs.jpcc.6b04429
40. Shamsheera, K. O., Anupama, R. P., Abraham, J. (2020). Computational simulation, surface characterization, adsorption studies and electrochemical investigation on the interaction of guar gum with mild steel in HCl environment. Results in Chemistry, 2, 100054. doi: https://doi.org/10.1016/j.rechem.2020.100054
41. Noorbakhsh Nezhad, A. H., Davoodi, A., Mohammadi Zahrani, E., Arefinia, R. (2020). The effects of an inorganic corrosion inhibitor on the electrochemical behavior of superhydrophobic micro-nano structured Ni films in 3.5% NaCl solution. Surface and Coatings Technology, 395, 125946. doi: https://doi.org/10.1016/j.surfcoat.2020.125946
42. Li, H., Zhang, B., Li, Y., Wu, P., Wang, Y., Xie, M. (2022). Effect of novel green inhibitor on corrosion and chemical mechanical polishing properties of cobalt in alkaline slurry. Materials Science in Semiconductor Processing, 146, 106691. doi: https://doi.org/10.1016/j.mssp.2022.106691
43. Bhardwaj, N., Sharma, P., Guo, L., Dagdag, O., Kumar, V. (2022). Molecular dynamic simulation and Quantum chemical calculation of phytochemicals present in Beta vulgaris and electrochemical behaviour of Beta vulgaris peel extract as green corrosion inhibitor for stainless steel (SS-410) in acidic medium. Colloids and Surfaces A: Physicochemical and Engineering Aspects, 632, 127707. doi: https://doi.org/10.1016/j.colsurfa.2021.127707
44. Subekti, N., Soedarsono, J. W., Riastuti, R., Sianipar, F. D. (2020). Development of environmental friendly corrosion inhibitor from the extract of areca flower for mild steel in acidic media. Eastern-European Journal of Enterprise Technologies, 2 (6 (104)), 34–45. doi: https://doi.org/10.15587/1729-4061.2020.197875
45. Pramana, R. I., Kusumastuti, R., Soedarsono, J. W., Rustandi, A. (2013). Corrosion Inhibition of Low Carbon Steel by Pluchea Indica Less. in 3.5% NaCL Solution. Advanced Materials Research, 785-786, 20–24. doi: https://doi.org/10.4028/www.scientific.net/amr.785-786.20
46. Wan, S., Chen, H., Liao, B., Guo, X. (2021). Adsorption and anticorrosion mechanism of glucose-based functionalized carbon dots for copper in neutral solution. Journal of the Taiwan Institute of Chemical Engineers, 129, 289–298. doi: https://doi.org/10.1016/j.jtice.2021.10.001
47. Hsissou, R., Dagdag, O., Abbout, S., Benhiba, F., Berradi, M., El Bouchti, M. et. al. (2019). Novel derivative epoxy resin TGETET as a corrosion inhibition of E24 carbon steel in 1.0 M HCl solution. Experimental and computational (DFT and MD simulations) methods. Journal of Molecular Liquids, 284, 182–192. doi: https://doi.org/10.1016/j.molliq.2019.03.180

48. Lebrini, M., Lagrenée, M., Vezin, H., Traisnel, M., Bentiss, F. (2007). Experimental and theoretical study for corrosion inhibition of mild steel in normal hydrochloric acid solution by some new macrocyclic polyether compounds. Corrosion Science, 49 (5), 2254–2269. doi: https://doi.org/10.1016/j.corsci.2006.10.029
49. Chauhan, D. S., Quraishi, M. A., Srivastava, V., Haque, J., ibrahimi, B. E. (2021). Virgin and chemically functionalized amino acids as green corrosion inhibitors: Influence of molecular structure through experimental and in silico studies. Journal of Molecular Structure, 1226, 129259. doi: https://doi.org/10.1016/j.molstruc.2020.129259
50. Shao, H., Yin, X., Zhang, K., Yang, W., Chen, Y., Liu, Y. (2022). N-[2-(3-indolyl)ethyl]-cinnamamide synthesized from cinnamomum cassia presl and alkaloid tryptamine as green corrosion inhibitor for Q235 steel in acidic medium. Journal of Materials Research and Technology, 20, 916–933. doi: https://doi.org/10.1016/j.jmrt.2022.07.122
51. Fekkar, G. et. al. (2020). Eco-friendly chamaerops humilis l. Fruit extract corrosion inhibitor for mild steel in 1 M HCL. International Journal of Corrosion and Scale Inhibition. doi: https://doi.org/10.17675/2305-6894-2020-9-2-4
52. Gautam, A., Siva, T., Sathiyanarayanan, S., Gobi, K. V., Subasri, R. (2022). Capped inhibitor-loaded halloysite nanoclay-based self-healing silica coatings for corrosion protection of mild steel. Ceramics International, 48 (20), 30151–30163. doi: https://doi.org/10.1016/j.ceramint.2022.06.288
53. Fan, J., Zhao, Z., Ding, Z., Liu, J. (2018). Synthesis of different crystallographic FeOOH catalysts for peroxymonosulfate activation towards organic matter degradation. RSC Advances, 8 (13), 7269–7279. doi: https://doi.org/10.1039/c7ra12615h
54. Farahati, R., Ghaffarinejad, A., Rezania, H. (Jafar), Mousavi-Khoshdel, S. M., Behzadi, H. (2019). Sulfonated aromatic polyamide as water-soluble polymeric corrosion inhibitor of copper in HCl. Colloids and Surfaces A: Physicochemical and Engineering Aspects, 578, 123626. doi: https://doi.org/10.1016/j.colsurfa.2019.123626
55. Ramakrishnan, K., Karthikeyan, S., Rajagopal, D. (2022). 2-Methoxy-4-(4-(((6-nitrobenzothiazol-2-yl)amino)methyl)-1-phenyl-1H-pyrazol-3-yl) phenol as powerful anti-corrosion inhibitor substantiated by Langmuir adsorption studies. Materials Letters, 313, 131823. doi: https://doi.org/10.1016/j.matlet.2022.131823
56. Ullah, S., Bustam, M. A., Assiri, M. A., Al-Sehemi, A. G., Gonfa, G., Mukhtar, A. et. al. (2020). Synthesis and characterization of mesoporous MOF UMCM-1 for CO_2/CH_4 adsorption; an experimental, isotherm modeling and thermodynamic study. Microporous and Mesoporous Materials, 294, 109844. doi: https://doi.org/10.1016/j.micromeso.2019.109844
57. Kundu, S., Gupta, A. K. (2006). Arsenic adsorption onto iron oxide-coated cement (IOCC): Regression analysis of equilibrium data with several isotherm models and their optimization. Chemical Engineering Journal, 122 (1-2), 93–106. doi: https://doi.org/10.1016/j.cej.2006.06.002
58. Swenson, H., Stadie, N. P. (2019). Langmuir's Theory of Adsorption: A Centennial Review. Langmuir, 35 (16), 5409–5426. doi: https://doi.org/10.1021/acs.langmuir.9b00154